Analysis of the singular vectors of the full-physics FSU Global Spectral Model

Zhijin Li

School of Computational Science and Information Technology

Florida State University, Tallahassee, Florida,32306,USA

I. M. Navon*†

Department of Mathematics and

School of Computational Science and Information Technology

Florida State University, Tallahassee, Florida,32306,USA

M. Y. Hussaini

School of Computational Science and Information Technology

Florida State University, Tallahassee, Florida,32306,USA

October 20, 2004

*Corresponding author, e-mail:navon@csit.fsu.edu

†Research sponsored by the NSF, Grant # ATM-9731472

Abstract

Analysis of singular vectors (SV) is performed on the Florida State University Global Spectral Model (FSUGSM) which includes linearized full physics of the atmosphere. It is demonstrated that the physical processes, especially precipitation, fundamentally affect the leading SVs. When the SVs are coupled with the precipitation geographically, their growth rates increase substantially and their structures change significantly. The physical processes however have little impact on growth rates or structures of the SVs that are geographically independent of precipitation. Furthermore, it is shown that spatial filtering along with the projection operator that projects the flow winds to the rotational wind (designed as a simple initialization process) improves the structural features of SVs and is found to mitigate spurious modes.

1 Introduction

In the 1960's Lorenz (1965) introduced singular vector (SV) analysis in meteorology to compute the largest error growth rates and estimate the atmospheric predictability of an idealized model. However, singular vector analysis was carried out for the realistic meteorological problems only in the late 1980's, a major obstacle being the huge computational expense. At the beginning of the 1990's, with the advent of adjoint techniques for the computation of SVs in meteorological problems (Molteni and Palmer, 1993; Mureau et al., 1993), the SV analysis for the sophisticated atmospheric general circulation models (GCMs) became feasible. SV analysis has since found applications in the areas of initial conditions for ensemble forecasting (Mureau et al., 1993; Molteni et al. 1996), of error-growth estimation in numerical weather prediction and atmospheric predictability (Molteni and Palmer, 1993; Ehrendorfer and Tribbia, 1997) and of adaptive observation strategy for ensemble forecasting (Lorenz and Emanuel, 1998; Palmer et al., 1998; Gelaro et al., 1998, Buizza and Montani, 1999; Puri et al., 2000). Thus the SV analysis has become as commonplace as normal mode analysis in the study of atmospheric flow instability (e.g., Farrell, 1988, 1989; Borges and Hartmann, 1992; Molteni and Palmer, 1993; Li and Ji, 1996, 1997; Oortwijn, 1998; De

Pondeca et al., 1998). Even so the most successful application of SV analysis appears to be in generating the initial conditions for ensemble forecasts.

The SV analysis for the numerical weather prediction models has been the subject of numerous studies. For the barotropic atmosphere, there are investigations by Borges and Hartmann (1992), Molteni and Palmer (1993) and Li and Ji (1996, 1997), to mention a few. The ECMWF has investigated the impact of model physics, resolution and atmospheric states on the feature of SVs for the atmospheric general circulation model ECMWF GCM (Buizza, 1994; Buizza and Montani, 1999; Buizza and Palmer, 1995; Mahfouf, 1999; Barkmeijer et al., 2001; Puri et al., 2001). Also, NCAR has examined the influence of moist physics on the SVs in the mesoscale model NCAR MM4 (Ehrendorfer et al., 1999). The research efforts at both ECMWF and NCAR have shown that the physical processes, in particular the boundary layer and moist physics, have a substantial impact on SVs. As the physical parameterization dramatically differs among different GCMs (while the dynamical part is generally similar), further examination of such observations in the frame work of other models is warranted. The objective of our present work is to study this problem in the context of FSUGSM, which has been used in numerical weather prediction for operational purposes for more than a decade. This model incorporates the physics of tropical meteorology.

As the SVs are computed by optimizing the growth of linear perturbations of the state trajectory, a persistent problem is the appearance of spurious modes. Buizza (1994) was the first to notice that such modes existed near and within the planetary boundary layer and decayed fast during the integration of the nonlinear model. He called them non-meteorological modes and he suggested the introduction of boundary-layer physics into the linearized model should suppress them. Barkmeijer et al. (2001) also observed similar modes in the tropical upper troposphere and they showed that they were inertia waves that grew only in the linearized model. These spurious modes are distinct from known meteorological modes. We observe that the linearization can also lead to a spuriously large growth rate and a spuriously distorted structure of the leading SVs even though they essentially consist of meteorological modes. This is a significant issue for predictability estimation and ensemble forecasting. Mitigation of the spurious effect of linearization on leading SVs is the key issue addressed in this work.

There are essentially two ways one could deal with the spurious modes. In the first approach, one adjusts the physical model parameters or modifies model physics. Such an approach was adopted by Buizza (1994) and Barkmeijer et al. (2001), who introduced boundary-layer physics and increased the value of the dissipation parameters in the vertical direction. In the second approach, one projects the variables used to compute the SVs onto a subspace that excludes spuriously growing modes. For example, one projects the wind velocity onto the rotational component; in other words, the divergent component of wind velocity is suppressed (Errico, 2000a, b). In view of the fact that spurious modes are localized at specific vertical model levels, Barkmeijer et al. (2001) noted the possibility of suppressing these modes by defining the variables for the computation of SVs on the model levels excluding those where the spurious modes appear.

A physically sound method for suppressing spurious modes is to introduce an initialization procedure that filters out the spuriously growing modes in the initial conditions (Haltiner and Williams, 1980). However, an operational initialization procedure is computationally demanding and hence could not be used directly in the computation of SVs, which requires multiple iterations. One may conjecture that to suppress spurious modes would require design of a filter that has the advantageous feature of an initialization procedure while allowing efficient computation. However the experience of Montani and Thorpe (2002) shows that this does not prevent the SVs from having unbalanced features. We propose a generalized filter which is a product of the projection operator of Barkmeijer (that projects onto a specified area) and a filter operator (that filters out either spatial scales or temporal scales or both, thereby mitigating or precluding spurious modes). Spatial filters have been used to investigate the effect of spatial scales on linear growth rate of SVs (Hartmann, et al., 1995) as well as balance constraints. Such a filter operator can also be identified with the projection operator of Errico (2000a, b) that projects the wind velocity field onto its rotational component. We show in this work that combining a low pass filter (that suppresses high wavenumbers) with some balance constraints effectively suppresses spurious modes, and more importantly improves the features of computed SVs.

Another aspect is related to the scheme of convective parameterization used in our experiments, i.e., the modified Kuo (1974) scheme instead of the relaxed Arakawa Schubert (1974) scheme(see Moorthi and Suarez (1992)) used in similar studies.

Hansen and Smith (2000) point out that in the presence of model error, the usefulness of SVs for adaptive observations is limited to the case when the linearity assumption as mentioned in their paper is valid, i.e., model linearization about the analysis requires the analysis error to be sufficiently small. In particular Section 3 of their paper is relevant. Li and Navon (2002) carried out such a careful verification.

The issue about successful application of SVs in general and the abovementioned issues raised in Smith (2000) and Hansen and Smith (2000) related to explicitly accounting for the dynamical evolution of uncertainty are valid issues and depend on the relative magnitude of operational analysis errors.

A recent work by Coutinho et al. (2004) presents a somewhat different perception about the impact of the inclusion of a full linearized physical parameterization package on extratropical SVs using the ECMWF integrated forecasting system. The crucial ingredient in the full package turns out to be the large-scale latent heat release. Some of the moist SVs occur at new locations and have tighter structures.

The paper is organized as follows. After a general introduction in the current Section 1, the FSUGSM and its linearization are briefly described in Section 2. A basic derivation of the general expressions for computations of SVs is presented in Section 3. The impact of physical processes on SVs is discussed in Section 4. The application of the generalized filter is described in Section 5. Finally, key results are discussed and summarized in Section 6.

2 Basic formulation of singular vector decomposition

For the sake of completeness, a brief description of the Florida State University Global Spectral Model (FSUGSM) is provided along with a succinct discussion of the singular vector decomposition.

2.1 The global spectral model

The FSUGSM has been used in operational weather forecasts for more than a decade. Forecasts based on this model emphasize tropical aspects such as monsoons and tropical storms (e.g., Krishnamurti, et al., 1991). This model has a comprehensive advanced physical parameterization package. The main physical parameterizations include a fourth-order horizontal diffusion (Kanamitsu et al., 1983), a modified Kuo-type convective scheme (Krishnamurti, et al. 1983), dry convective adjustment, large-scale condensation, surface flux via similarity theory (Businger, et al. 1971), vertical distribution of fluxes utilizing diffusive formulation where the exchange coefficients are functions of the Richardson number (Louis, 1979), long-wave and short wave radiative fluxes based on a band model (Harshvardan and Corsetti, 1984; Lacis and Hansen, 1974), computation of low, middle and high clouds based on threshold relative humidity for radiative calculation and surface energy balance coupled to the similarity theory (Krishnamurti et al., 1991).

The adjoint system of FSUGSM is a result of several years effort. The adjoint system includes the dynamic core (Wang, 1993) and all abovementioned physical parameterizations (Tsuyuki, 1996; Zhu and Navon, 1997). Both the tangent linear model and consequently the adjoint contain simplifications with respect to the nonlinear forecast model. This model has been successfully applied to carry out both 4D-Var and optimal parameter estimation (Zhu and Navon, 1999; Tsuyuki, 1997; Li, et al. 2000).

In the following computations, the spectral expansion of the model variables is triangularly truncated at the wave number 42 (T42). A sigma (σ) coordinate is used in the vertical direction and the vertical resolution consists of 12 layers roughly between 100 and 1000 hPa.

2.2 SVD basics

Consider the FSUGSM, which is perturbed at any point in its nonlinear trajectory. The evolution of the perturbation state vector x is then governed by

$$x_t = A(t,0)x_0, \tag{1}$$

where x_t is the perturbation at time t, x_0 is the initial perturbation at time 0, and $A(t,0)$ is the resolvent or forward tangent propagator from time 0 to time t. $A(t,0)$ is a linearized

version of the original nonlinear operator. The equation (1) is usually called the tangent linear model. In the present case, the perturbation state vector x represents $\{u, v, T, \ln \pi\}$, which are the perturbations of velocity components, temperature, and logarithm of surface pressure respectively.

In order to compute the fastest growing perturbations (the so-called singular vectors that will be defined precisely later), it is necessary to define an inner product for the linear vector space of perturbations. We define the inner product, $(x, y) =< x, Ey >$, where $< .;. >$ denotes a Euclidean scalar product and E denotes a weight matrix, so that it yields the norm,

$$||x||^2 = (x, x) =< x, Ex >= \frac{1}{2} \int_0^1 \int_\Sigma \left[u^2 + v^2 + \frac{c_p}{T_r} T^2 \right] (\frac{\partial p}{\partial \sigma}) d\Sigma d\sigma + \frac{1}{2} \int_\Sigma R_d T_r P_r (ln\pi)^2 d\Sigma. \tag{2}$$

Here, C_p is the specific heat of dry air at constant pressure, R_d the gas constant for dry air, $T_r = 300K$ a reference temperature, $P_r = 800hpa$ a reference pressure. E is obviously a positive-definite diagonal matrix. This norm (2) does not include the latent heat of condensation (Mahfouf et al., 1996; Ehrendorfer et al., 1999) and is called the dry total energy norm. As pointed out by (Buizza and Palmer, 1995) such a norm permits reverse energy cascade from subsynoptic to synoptic scales. Molteni et al., (1996) observe that in the absence of complete analysis-error covariance, the total energy norm is the most appropriate for ensemble prediction. Its physical relevance and importance is due to the fact that it includes kinetic, thermal and potential energies. We did not include moisture in the norm as there is at present a certain arbitrariness in modeling specific humidity (Mahfouf and Buizza, 1996).

In the discrete case pertaining to FSUGSM under study, the perturbation state vector $x = \{u, v, T, \ln \pi\}$ is of dimension $M = I * J * (3K + 1)$ where I, J and K are the number of degrees of freedom in the longitudinal (i), latitudinal (j) and vertical (k) directions. The matrix A is $M * M$, real and nonsingular. The matrix E in the weighted inner product is diagonal, positive definite and it has the form,

$$\begin{aligned} \mathbf{E} \;=\; & diag\{\cdots, w(j)p_s(i,j)\delta\sigma(k)\delta\lambda, \cdots, \cdots, w(j)p_s(i,j)\delta\sigma(k)\delta\lambda, \cdots, \\ & \cdots, w(j)p_s(i,j)\frac{c_p}{T_r}\delta\sigma(k)\delta\lambda, \cdots, \cdots, w(j)R_d T_r P_r \delta\lambda, \cdots\} \end{aligned} \tag{3}$$

where $\delta\lambda$ and $\delta\sigma(k)$ are the step sizes in the longitude and vertical directions respectively, and $p_s(i,j)$ the surface pressure. The Gaussian integration is used in latitude, and $w_(j)$ are the Gaussian weights.

The definition of the norm allows one to relate the energy of the perturbation x at time t to its initial value:

$$\frac{||x_t||^2}{||x_0||^2} = \frac{< x_t, E_t x_t >}{< x_0, E_0 x_0 >} = \frac{< Ax_0, E_t Ax_0 >}{< x_0, E_0 x_0 >} = \frac{< x_0, A^T E_t A x_0 >}{< x_0, E_0 x_0 >} = \lambda^2, \tag{4}$$

where the superscript T represents the transpose, and the subscripts t and 0 denote the weight matrix at time t and 0. In the present instance, $E_t = E_0$ and λ is usually called the energy amplification factor.

This suggests the generalized eigenvalue problem,

$$A^T E_t A v_i = \lambda_i^2 E_0 v_i. \tag{5}$$

$A^T E_t A$ is symmetric and positive definite and its eigenvalues can be ranked in the decreasing order: $\lambda_1 > \lambda_2 > \lambda_3 > ... > ... > 0$. The generalized eigenvectors v_i and the generalized eigenvalues λ_i are respectively called the singular vectors and singular values of A (with respect to E_0-norm). They are orthogonal and form a complete basis. Any x_t can therefore be expressed as a linear combination of the singular vectors v_i, and the amplification factor as a linear combination of the singular values λ_i. The leading singular vectors are sometimes called optimal perturbations and the time during which perturbation growth is considered the optimization time.

In practice, one can only compute a small number of singular vectors compared with the huge dimension of the model variables. In order to make the singular vectors more relevant to limited area models, Barkmeijer (1992) introduced a local projection operator P, which sets model variables to zero outside the concerned area. Then the definition of the amplification factor (4) is generalized as

$$\lambda^2 = \frac{< Px_t, E_t P x_t >}{< x_0, E_0 x_0 >}. \tag{6}$$

This projection operator has been used extensively in SV analysis (e.g., Barkmeijer, 1992; Buizza et al., 1996). Pursuing this line of argument, one can further introduce a filter

operator F and generalize (6) as

$$\lambda^2 = \frac{< PF_t x_t, E_t PF_t x_t >}{< F_0 x_0, E_0 F_0 x_0 >}. \tag{7}$$

If F_t and F_0 transform the complete wind field to the rotational field (i.e., filters out the potential component), they could be identified with the projection operator discussed by Errico (2000a, b). In the following computations, F will be a temporal or spatial filter combined with other constraints, aimed at suppressing spurious modes in leading singular vectors and at improving their features.

Consistent with the generalized definition of amplification factor (7), the eigenvalue problem becomes

$$A^T F_t^T P^T E_t P F_t A v = \lambda^2 F_0^T E_0 F_0 v. \tag{8}$$

Obviously, $A^T F_t^T P^T E_t P F_t A$ and $F_0^T E_0 F_0$ are positive semi-definite matrices. The singular vectors and singular values have the same properties as those for the definition (4), but singular vectors are orthonormal and complete with respect to $F_0^T E_0 F_0$.

When the adjoint operators A^T, F^T and P^T are available, the eigenvalue problem (8) can be solved even for a sophisticated GCM by using Lanczos-type algorithms. These algorithms require only the evaluation of matrix-vector products and circumvent the computationally expensive explicit manipulations of those large matrices. There are quite a few software packages based on Lanczos type algorithms. We use the ARPACK software package that was developed specifically for problems of large dimensions (Lehoucq et al., 1998).

3 Singular vectors without filtering

We examine the characteristics of SVs without filtering to establish the reference for the effect of filtering. The projection operator confines the domain of computation of the energy norm (2) to the Northern hemisphere. The optimization time interval is taken as 36h. We analyze the leading 10 SVs, as their singular values decrease relatively quickly in comparison with the later singular values when the time window is 24h (as also observed by Buizza 1994).

In the linearized model, the basic state is a model forecast, which starts from the initialized analysis valid at 00UTC 03 September 1996, using the full-physics model. Fig. 1 shows the zonal wind component of the initial condition at 300 hPa and the 36h accumulated precipitation of the forecast. The perturbation of the basic state, which constitutes leading SVs is mostly located on the southern flank of the jets and their exit areas (not shown in the figure) as pointed by Buizza and Palmer 1995 and Hoskins et al. 2000.

3.1 Model without physics

In the present context, the model without physics comprises the dynamic core with simple horizontal diffusion and surface drag (Case NP). For this model, we find that seven of the ten leading SVs are dominated by the spurious modes, which are characterized by the vertical and horizontal perturbations with two-grid size wavelength. As an example, Fig. 2 presents the horizontal structures at 800 hPa and the vertical-height section structure of the first SVs. Such structures have also been identified in the ECMWF model by Buizza (1994). The three-point spatial scale of the spurious modes suggests the possibility of suppressing them by spatial filtering discussed in the next section.

The three SVs that appear to be "meteorological" in the sense of Buizza et al. (1993) are the 7th, 9th and 10th. For instance, the horizontal and vertical structures of the 10th SV are plotted in Fig. 3, which shows its major perturbations are located in the southern flank of the Asia Jet. Zeng (1983) argues that the perturbation extracts barotropic energy from the basic jet stream as seen in the horizontal structure in (Fig. 1). Hoskins et al. (2000) and Barcilon and Bishop (1998) explain that the vertical structure is a typical mid-latitude baroclinically growing non-normal mode. In the following, we identify the " meteorological" modes by visually examining their vertical and horizontal structures and only those showing horizontal connected structures and vertical perturbations deeper than four vertical model levels are considered as reasonable modes.

3.2 Model with the boundary layer physics

We first include the boundary layer physics and vertical diffusion in the model (Case BP). In order to compare the SVs from Case NP and Case BP, we follow Buizza et al. (1993), Buizza (1994) and compute the so-called projection matrix:

$$m_{ij}(NP, BP) = (< v_i(NP); Ev_j(BP) >)^2.$$

Each element of the projection matrix is the squared scalar product of the i-th SV of the case NP and the j-th SV of the case BP. As such it represents the amount of energy of the i-th SV of the NP case that is explained by the j-th SV of the BP case. The sum of the matrix elements with a fixed index represents how well the i-th SV of the NP case can be reconstructed from a linear combination of the first N SVs of the BP case.

A measure of similarity based on projection of a set of SVs on another is provided by the similarity index of the two cases NP and BP and is defined as:

$$s(A, B; N) = \frac{1}{N} \sum_{i,j=1}^{N} m_{i,j}(A, B),$$

(which measures the similarity between the unstable subspaces spanned by the first N SVs of each case). The index equals unity if the unstable subspaces of the two cases are identical.

The projection matrix (Table 1), shows that the 7th SV of Case NP resembles the 4th SV of Case BP, the 9th SV of Case NP resembles the 7th SV of Case BP, and the 10th SV of Case NP resembles the 8th SV of Case BP. These three SVs are the "meteorological" ones in the sense of Buizza et al. (1993) for Case NP. In Case BP, the 10th SV is also "meteorological" in the same sense. We observe that the incorporation of the boundary-layer physics and the vertical diffusion leads to limited improvement in the structure of the SVs; while the three SVs from the case with no physics persist in the present case, an additional reasonable SV (tenth SV) appears, but there are still six SVs that are spurious. Our observation is similar to that of Buizza (1994).

3.3 Model with the full physics

In the following, we incorporate all the physical processes in the nonlinear model as described in section 2a into the adjoint model (Case FP) and show that it leads to a substantial improvement of SVs.

Fig. 4 presents the vertical and horizontal structures of the 6th SV, which may be viewed as representative of the three SVs consisting of tropical modes. The major perturbations are geographically co-located with the major tropical precipitation areas. In the vertical direction, the structure of the 6th SV is localized mainly in the upper model and middle-lower model levels. The upper part is characterized by a slight tilt toward the east and is understood to be associated with an easterly baroclinic structure. The middle-lower level part is generally understood to have a barotropic structure. Such structure features distinguish these tropical modes from the spurious barotropic and inertial unstable modes that have been comprehensively analyzed by Barkmeijer et al (2000). However, these three SVs are contaminated to some degree by inertial unstable modes, as indicated by the perturbation centers located between $200hPa$ and $300hPa$.

As expected, all the three reasonable SVs obtained for both the NP and BP cases are the leading SVs for Case FP. This is evidenced by the values of projection matrix entries amongst the three cases being larger than 80% in the projection matrix (not shown). The new leading SVs include the tropical modes discussed above and also new leading SVs which are mainly located over the Atlantic Ocean as shown in Fig. 5.

Thus, the full physics model is found to suppress rather effectively the spurious modes, which may possibly be a common feature of all GCMs with full physics. This is due to i) the surface energy flux, boundary layer physics and vertical diffusion being treated in a consistent manner, and ii) some physical processes, such as the dry convective adjustment and radiative transfer, playing an energy diffusion role.

We observe that the full physics model brings forth the tropical modes among the leading SVs. Then a natural question arises as to the impact of the full physics model on the SVs that are mainly located at mid-latitudes and higher latitudes. In order to answer this question, we compute these SVs while the projection operator is defined over the area north of $30°N$.

Then the projection matrix, as defined before, is computed for comparing the cases for 30°N and the Northern Hemisphere. The three SVs consisting of tropical modes,(i.e., the 2nd, 3rd and 6th SV of Case FP), are not present in the case for 30°N, as indicated by the zero value of the indices (Table 3). There are three SVs, that is, the 4th, 5th and 10th of Case FP that are present in the case for 30°N. These three SVs are also obtained in Case NP and Case BP. Thus, those three SVs are not affected by the physical processes.

Now we analyze the effect of the inclusion of the full physics on the singular values (Table 2). The three SVs located in mid-latitudes present in all the three cases of Case NP, Case BP, and Case FP, respectively, have close singular values. This implies that the model physical processes have little impact on the singular values of these SVs.

In contrast, precipitation significantly increases the growth rate of the SVs when their modes are located in the tropics. Here we do not suggest that there are new modes excited solely by precipitation, since these modes are evidently baroclinic. The combination of the baroclinity and precipitation latent heating leads those modes to larger singular values and then they become leading SVs. The conclusion here is that the precipitation enhances growth rates of SVs only when they geographically overlap with precipitation areas.

These results concur with results obtained by Errico et al. (2000) pointing that the primary effect of considering moist physics in the model leads to faster growth of perturbations than in the dry situation. (see also Ehrendorfer et al. 1999). The important point made by Errico and Ehrendorfer is that moist physics in the linear models enables new instability mechanisms to be triggered, leading to new SV structures. This can be seen from the first singular value for all the three cases (Table 2).

4 Dynamically filtered singular vectors for the full physics model

The inclusion of the full physics has substantially improved the computation of SVs as it has to a great degree suppressed the spurious modes and also enhanced the growth of the modes present in the leading SVs. However, there still exist some deficiencies. For instance,

spurious modes have not been completely eliminated in the leading SVs, and SVs in Fig. 3a have horizontal spatial scales of only a few hundred km, which is smaller than typical synoptic scales.

The present filtering method involves the dynamics of the model and controls the computation of SVs. These filtering operators include both spatial and temporal filters, as well as the rotational projection used by Errico (2000a).

The spatial filter can be applied to initial condition, which then is equivalent to an initialization process. It can also be applied at the final time of the time window. The results are found to be insensitive to the filtering at the end of the time window. For example, F_t in (8) is a truncation operation that truncates the field at T15, and we find no measurable difference in the computed leading SVs.

Spurious modes are well suppressed in the computed leading SVs when we use the model with full physics and apply the spatial truncation at resolution T21 to the initial condition, as well as implement the projection of the wind fields onto the rotational projector Errico (2000a). Fig. 6 presents the first 10 square singular values for the leading 10 SVs for the optimization time window of 24-h. Those spurious modes with isolated small spatial scale perturbations do not exist in all the 10 leading SVs.

Let us further examine how the filtering affects the meteorological modes significantly. By examining the singular values, we have seen that those SVs consisting of the meteorological modes show the values to be reduced by about 50%. As expected, their structure has larger scales. The combined perturbations of all the ten SVs appear to cover the extra-tropics, which is desired by ensemble forecasts. It is interesting to note that all the reasonable meteorological SVs at middle latitudes in Case NP have comparable ones (in terms of both the geographical location and spatial structure) as indicated typically by the 1st, 4th and 9th SV. Those modes excited by physics in the tropics and subtropics in Case FP also have comparable ones, but only in terms of the geographical location. The tropical perturbation with filtering presents well-organized wave train structure as indicated by the 8th SV, which may be attributed to the use of only the rotational wind (see Errico 2000a, b).

As the computation of SVs is based on a linearized model, the role of filter in this situation is similar to that of turbulence, which is equivalent in a sense to diffusion that exerts stronger effect on perturbations of smaller scales than of larger scales.

When the time filter is applied, (6) is generalized as

$$\lambda^2 = \frac{\int_s^t < Px_\tau, E_\tau Px_\tau > d\tau}{(t-s) < x_0, E_0 x_0 >}. \tag{9}$$

Here, we take $t-s$ to be 6-h, while the optimization time interval is 36-h. The results indicate that such a filter relatively enhances spuriously growing modes. All the 10 SVs consist of non-meteorological modes for the Case NP. Since the spuriously growing modes are locally standing perturbations, they are not weakened by the time filtering. On the other hand, the meteorological modes which consist of traveling perturbations are weakened by the time filter.

5 Reexamination of moisture processes

The above discussion concerns the case where the basic state of the model forecast is obtained from an initialized analysis valid at 00UTC 03 Sep 96. A careful examination of Fig. 1 shows that the precipitation over the North Hemisphere is relatively weak, and is mostly located in the tropical area. We consider a new case (precipitation case) in which the linearization is carried out around the basic state of the model forecast obtained from the initialized analysis valid at 12UTC 24 June 1994 when the Indian Monsoon was active. The precipitation is stronger and it covers more extensive areas than in the first case. SVs are computed with filter, that is, the truncation at resolution T21 is applied to the initial condition, along with projecting the wind fields onto the rotational components (Errico, 2000a). Fig. 8 displays the first three leading SVs for the precipitation case. Fig. 9 is the same as Fig. 8, but for the case without moisture (NM).

This case confirms the conclusion about the effect of precipitation on SVs from the previous case. To single out the effect of precipitation, we further perform two experiments. One experiment uses the full physics, and the other turns off the moisture processes. The precipitation excites new SVs as in the previous case. The 8th SV in Fig. 7 is the precipitation

excited new SV, since it disappears when the moisture process is turned off (not shown). In Fig. 7, the four SVs of the 5th, 6th, 8th, and 10th have perturbations well overlapping with the monsoon precipitation areas, while the other two SVs of the 2nd and 3rd overlap with other precipitation areas. These six SVs have a comparable counterpart in the case without moisture process. We see that the moisture process leads to shift the perturbations of the six SVs toward equator, and their singular values are 30-50% larger than those without the moisture process. In contrast, the 7th SV has also a comparable counterpart in the case without the moisture process, and they have close singular values. These results are consistent with the conclusion that the precipitation enhances growth rates of SVs only when their perturbations geographically overlap with precipitation areas.

It should be pointed out that the 1st SV consists of spurious modes in this case. Its singular value is as large as 4.9×10^6. As this SV disappears when the moisture process is turned off, it may be attributed to the singularities inherent in modeling the moisture process, which has been well documented and described by Errico et al. (1999). The presence of this SV may point to the fact that applying wave truncation and dynamical balance restriction to the initial values is not able to remove spurious modes due to the discontinuities in the adjoint model when strong precipitation occurs.

6 Summary of results and conclusions

The present results are consistent with the observations of Ehrendorfer et al. (1999) and Barkmeijer et al. (2000) on the impact of physical processes on SVs. The impact of physics on SVs can be substantial in a global model even for an optimization time interval as short as 24h. The growth rates are significantly enhanced and the structures are significantly altered by the inclusion of physics. However, we have noticed that physical processes, especially precipitation, affect a leading SV fundamentally only when the SV perturbation is geographically coupled with precipitation. For those SVs that are geographically independent of precipitation, physics has little impact on either their growth rate or the structure. The impact of physics is characterized by localization. Actually, in our case, physics exerts little impact on the structure of the computed SVs when the projection operator is confined to

$30°N$, and this is simply due to the fact that precipitation occurs mainly in the tropics and subtropics and can not overlap with SV perturbations.

The FSUGSM model appears to have more leading SVs dominated by spurious modes than the ECMWF model (Buizza 1994). A possible reason may be that this version of the FSUGSM has a relatively low vertical resolution. Specifically, this version of FSUGSM has only 12 levels in the vertical direction, while ECMWF models have at least 19 levels.

Another reason is related to the scheme of moisture parameterization used in our experiments (i.e., modified Kuo (1974) scheme instead of the relaxed Arakawa Schubert (1974) scheme). Research work by De Witt (1996) has shown that integrations done with the RAS scheme better approximate the precipitation gradients in the tropics than when the Kuo scheme is used. We note that the spatial filter coupled with the operator that projects the flow winds to the rotational wind improves the structural features of the computed SVs and is beneficial in the suppression of spuriously growing modes. On the other hand, the temporal filter seems to enhance spurious modes as discussed in section 4.

The spatial filter plays a role similar to an initialization process in numerical weather prediction. Theoretically, an operational initialization procedure could be more reasonable and also feasible to implement. However, the computational cost of carrying out an operational initialization procedure during the computation of the SVs is prohibitively expensive. As evidenced by this study, a simple filtering procedure could play the role of an initialization procedure to some degree. When spatial filtering and some flow balance constraints are appropriately combined, we can expect a satisfactory filtering procedure for the computation of SVs. Further, this procedure can always be used to control the structure of SVs for mitigating the effect of linearization.

Note that the filtering process does not appear to affect the physical processes. However, it should be carefully verified in each instance, since geographical locations and growth rates of spurious modes are very sensitive to background flows and model physics. If one can not guarantee that the SVs are free of spurious modes, one risks drawing incorrect conclusions on the effect of physical processes due to the interference of spurious modes.

This study raises two research issues worth investigating. The first one is to verify the effectiveness and the benefit of the filtering technique in an operational setting such as an

ensemble forecast. The second issue is to investigate if the filtering technique still plays a useful role when the error covariance is introduced as discussed by Barkmeijer et al. (1998, 1999). Technically, the filtering process proposed in this study can still be implemented in such a case, but its usefulness may depend on the characteristics of the error covariance matrix.

The effect of moisture on the number of growing structures as well as the specification of appropriate norms to properly account for moist processes are issues that remain to be studied .

Acknowledgments

The second author would like to express his gratitude for the support extended to him by the Center of Excellence (COE) at Florida State University. The first and second authors also acknowledge support from NSF grants ATM-97B1472 managed by Dr. Pamela Stephens. and ATM-0201808 managed by Dr Linda Peng, who he would like to thank for their support.

The authors would like also to thank Dr Roberto Buizza of ECMWF for his expert comments and advice.

The expert in depth review of an anonymous reviewer improved markedly the presentation of the paper.

REFERENCES

Arakawa, A. and Schubert, W. H. 1974. Interaction of a cumulus ensemble with the large-scale environment. Part I.*J. Atmos. Sci.* **31**, 674-704.

Barcilon, A. and Bishop, C. 1998. Non-modal development of baroclinic waves undergoing horizontal shear deformation. *J. Atmos. Sci.*, *J. Atmos. Sci.* **55**, 3583-3597.

Barkmeijer, J. 1992. Local error growth in a barotropic model.*Tellus* **44A** , 314-323.

Barkmeijer, J., van Gijzen, M., Bouttier, F. 1998. Singular vectors and estimates of the analysis error covariance matrix. *Q. J. R. Meteor. Soc.* **124**, 1695-1713.

Barkmeijer, J., Buizza, R. and Palmer, T.N. 1999. 3D-Var Hessian singular vectors and their potential use in the ECMWF ensemble prediction system. *Q. J. R. Meteor. Soc.* **125**, 2333-2351.

Barkmeijer, J., Buizza, R., Palmer, T. N., Puri, K. and Mahfouf, J.-F. 2001. Tropical singular vectors computed with linearized diabatic physics.*Q. J. R. Meteorol. Soc.* **127**, 685-708.

Borges, M. D. and Hartmann, D. L. 1992. Barotropic instability and optimal perturbations of observed non-zonal flow. *J. Atmos. Sci.* **49**, 335-354.

Businger, J. A., Wyngard, J.C., Izumi, Y. and Bradley, E.F. 1971. Flux profile relationships in the atmospheric surface layer. *J. Atmos. Sci.* **28**, 181-189.

Buizza., R. 1994. Sensitivity of optimal unstable structures. *Q. J. R. Meteor. Soc.* **120**, 429-451.

Buizza., R. and Palmer, T. N. 1995. The singular vector structure of the global atmospheric global circulation. *J. Atmos. Sci.* **52**, 1434-1456.

Buizza, R. and Montani, A. 1999. Targeting observations using singular vectors. *J. Atmos. Sci.* **56**, 2965-2985.

Buizza, R., Tribbia, J., Molteni,F. and Palmer, T. N. 1993. Computation of optimal unstable structures for a numerical weather prediction model.*Tellus* **45A**, 388-407.

Buizza, R., Gelaro, R., Molteni, F. and Palmer, T. N. 1997. The impact of increased resolution on predictability studies with singular vectors. *Quart. J. Roy. Meteor. Soc.* **123**, 1007-1033.

Coutinho, M. M., Hoskins, B. J. and Buizza, R. 2004. The influence of physical processes on extratropical singular vectors. *J. Atmos. Sci.* **61**, 195-209.

de Pondeca, M. S.F.V., Barcilon, A. and Zou, X. 1998. An adjoint sensitivity study of the efficacy of modal and non-modal perturbation in causing model block onset. *J. Atmos. Sci.* **55**, 2095-2118.

DeWitt, D. 1996. The Effect of the Cumulus Convection on the Climate of the COLA General Circulation Model. COLA Technical Report No. 27, Center for Ocean-Land-Atmosphere Studies, Calverton, MD 20705,USA.

Ehrendorfer, M. and Tribbia, J. J. 1997. Optimal prediction of forecast error covariance through singular vectors. *J. Atmos. Sci.* **54**, 286-313.

Ehrendorfer, M., Errico, R. M. and Raeder, K. D. 1999. Singular vector perturbation growth in a primitive equation model with moist physics. *J. Atmos. Sci.* **56**, 1627-1648.

Errico, R. M. and Raeder, K. D. 1999. An examination of the accuracy of the linearization of a mesoscale model with moist physics. *Quart. J. Roy. Meteorol. Soc.* **125**, 169–195.

Errico, R. M. 2000a. Interpretations of the total energy and rotational energy norms applied to determination of singular vectors. *Quart. J. Roy. Meteorol. Soc.* **126**, 1581-1599.

Errico, R. M. 2000b. The dynamical balance of leading singular vectors in a primitive-equation model. *Quart. J. Roy. Meteorol. Soc.* **126**, 1601-1618.

Errico, R. M.,Ehrendorfer, M. and Raeder, K. D. 2001. The spectra of singular values in a regional model. *Tellus* **53A**,317-332.

Farrell, B. F. 1988. Optimal excitation of neutral Rossby waves. *J. Atmos. Sci.* **45**, 163-172.

Farrell, B. F. 1989. Optimal excitation of baroclinic wave. *J. Atmos. Sci.* **46**, 1193-1206.

Gelaro, R., Buizza, R., Palmer, T. N. and Klinker, E. 1998. Sensitivity analysis of forecast errors and the construction of optimal perturbations using singular vectors. *J. Atmos. Sci.* **55** 1012-1037.

Haltiner, G. J. and Williams, R. T. 1980. Numerical Prediction and Dynamic Meteorology, Second Edition, John Wiley and Sons, New York, 477pp.

Hansen, J.A. and Smith A. Leonard 2000. The role of operational constraints in selecting supplementary observations. *J. Atmos. Sci.* bf 57 2859-2871.

Harshvardan, R. and Corsetti, T. G. 1984. Long-wave parameterization for the UCLA/GLAS GCM. *NASA Tech. Memo. 86072, Goddard Space Flight Center*, Greenbelt, MD 20771, 52 pp.

Hartmann, D.L., Buizza, R. and Palmer, T. N. 1995. Singular vectors: the effect of spatial scale on linear growth of disturbances. *J. Atmos. Sci.* **52**, 3885-3894.

Hoskins, B. J., Buizza, R. and Badger J. 2000. The nature of singular vector growth and structure. *Quart. J. Roy. Meteorol. Soc.* **126**, 1565-1580.

Kanamitsu, M., Tada, K., Kudo, K., Sato, N. and Isa, S. 1983. Description of the JMA operational spectral model. *J. Met. Soc. Japan* **61**, 812-828.

Krishnamurti, T. N., Xue, J., Bedi, H. S., Ingles, K. and Oosterhof, D. 1991. Physical initialization for numerical weather prediction over the tropics. *Tellus* **43A**, 53-81.

Krishnamurti, T. N., Bedi, H. S. and Ingles, K. 1993. Physical initialization using the SSM/I rain rates. *Tellus* **45A**, 247-269.

Kuo, H.-L. 1974. Further studies of the parameterization of the influence of cumulus convection on large-scale flow. *J. Atmos. Sci.* **31**, 1232-1240.

Lacis, A. A. and Hansen, J. E. 1974. A parameterization of the absorption of solar radiation in the earth's atmosphere. *J. Atmos. Sci.* **31**, 118-133.

Lehoucq, R. B., Sorensen, D. C. and Yang, C. 1998. ARPACK Users' guide: solution of large-scale eigenvalue problems with implicitly restarted Arnoldi methods. *Series: Software, Environments, and Tools* 6, SIAM, Philadelphia 160 pp.

Li, Z and Ji, L. 1996. Internal dynamics of the generation of atmospheric teleconnection patterns. *Adv. Atmos. Sci.* **13**, 19-32.

Li, Z. and Ji, L. 1997. Efficient forcing and teleconnection patterns. *Quart. J. Roy. Meteorol. Soc.* **123**, 2401-2423.

Li, Z., Navon, I. M. and Zhu Y. 2000. Performance of 4D-Var with different strategies on the use of adjoint physics with the FSU Global Spectral Model. *Mon. Wea. Rev.* **128** , 668-688.

Liu, Z. and Navon I. M. 2002 Documentation of the Tangent Linear and Adjoint Models of New MPI Version of the FSU Global Spectral Model . Technical Report (2002).39pp. Available from `http://www.csit.fsu.edu/~navon/pubs/`

Lorenz, E. N. 1965. A study of the predictability of a 28 variable atmospheric model. *Tellus* **17**, 321-333.

Lorenz, E. N. and Emanuel, K. A. 1998. Optimal sites for supplementary observations: simulation with a small model. *J. Atmos. Sci.* **55**, 399-414.

Louis, J. -F. 1979. A parametric model of vertical eddy fluxes in the atmosphere. *Boundary Layer Meteorology* **17**, 187-202.

Mahfouf, J.-F. 1999. Influence of physical processes on the tangent-linear approximation. *Tellus* **51A**, 147-166.

Mahfouf, J.-F., Buizza, R. and Errico, R. M. 1996. Strategy for including physical processes in the ECMWF variational data assimilation system. Proc. 1996 ECMWF Seminar on Data Assimilation and Workshop on Non-Linear Aspects of Data Assimilation, ECMWF, 595-632. [Available from ECMWF, Shinfield Park, Reading, Berkshire RG2 9AX, United Kingdom.]

Mahfouf, J.-F. and Rabier, F. 1998. The ECMWF operational implementation of four-dimensional variational assimilation. Part II: Experimental results with improved physics. *Q. J. R. Meteorol. Soc.* **126**, 1171-1190.

Molteni, F. and Palmer, T. N. 1993. Predictability and finite-time instability of the northern winter circulation.*Q. J. Roy. Meteorol. Soc.* **119**, 269-298.

Molteni, F., Buizza, R., Palmer, T. N. and Petroliagis, T. 1996. The new ECMWF ensemble prediction system: methodology and validation. *Quart. J. Roy. Meteorol. Soc.* **122**, 73-119.

Montani A. and Thorpe, A. J. 2002: Mechanisms leading to singular vector growth for FASTEX cyclones,*Quart. J. Roy. Meteorol. Soc.*, **128**, 131-148 .

Moorthi, S. and Suarez, M. 1992. Relaxed Arakawa-Schubert: A parameterization of moist convection for general circulation models. *Mon. Wea. Rev.* **120**, 978-1002.

Mureau, R., Molteni, F. and Palmer, T. N. 1993. Ensemble prediction using dynamically-conditioned perturbations. *Quart. J. Roy. Meteorol. Soc.* **119**, 299-323.

Oortwijn, J. 1998. Predictability of the onset of blocking and strong zonal flow regimes. *J. Atmos. Sci.* **55**, 973-994.

Palmer, T.N., Gelaro, R., Barkmeijer, J. and Buizza, R. 1998. Singular vectors, metrics, and adaptive observations. *J. Atmos. Sci.* **55**, 633-653.

de Pondeca, M. S.F.V., Barcilon, A. and Zou, X. 1998. An adjoint sensitivity study of the efficacy of modal and non-modal perturbation in causing model block onset. *J. Atmos. Sci.* **55**, 2095-2118.

Puri, K., Barkmeijer J. and Palmer, T. N. 2001. Ensemble prediction of tropical cyclones using targeted diabatic singular vectors. *Quart. J. Roy. Meteor. Soc.* **127 (572)**, 709-731 .

Smith, L.A. 2000. Disentangling uncertainty and error:on the predictability of nonlinear systems.In In: Nonlinear Dynamics and Statistics, A. Mees (ed.), Birkhauser, 2000 41-68.

Toth, Z. and Kalnay, E. 1997. Ensemble forecasting at NCEP and the breeding method. *Mon. Weather. Rev.* **125**, 3297-3319.

Tsuyuki, T. 1996. Variational data assimilation in the tropics using precipitation data. Part II: 3-D model. *Mon. Wea. Rev.* **124**, 2545-2561.

Tsuyuki, T. 1997. Variational data assimilation in the tropics using precipitation data .3. Assimilation of SSM/I precipitation rates *Mon. Wea. Rev.*,**125**, 1447-1464.

Wang, Z. 1993. Variational data assimilation with 2-D shallow water equations and 3-D FSU Global Spectral Models, *Ph. D. Dissertation*, Department of Mathematics, The Florida State University, 235 pp.

Zhu, Y. and Navon, I. M. 1997. Documentation of the tangent-linear and adjoint models of the radiation and boundary layer parameterization packages of the FSU Global Spectral Model T42L12. *Tech. Report*, FSU-SCRI-97-98.

Zhu, Y. and Navon, I. M. 1999. Impact of parameter estimation on the performance of the FSU Global Spectral Model using its full-physics adjoint. *Mon. Wea. Rev.* **Vol.127, No.7** ,1497-1517.

Zeng, Q.-C. 1983. The evolution of a Rossby-wave Package in a three-dimensional baroclinic atmosphere. *J. Atmos. Sci.* **40**, 73-86.

Figure Captions

Fig. 1. (a) Zonal wind analysis at 300hPa and valid at 00UTC 03 September 1996. The contour interval is $10.0m$, and negative values are dashed and values larger than $30.0m$ shaded. (b) Accumulated precipitation of the forecast over 36-h. The contour interval is $10.0mm$, and values larger than 30.0 mm are shaded.

Fig. 2 The 1st SV of the case where only simple horizontal diffusion and the surface drag are included in the model physics and with an optimal time interval of 36-h. (a)

The streamfunction at 800 hPa, and (b) the longitude-model level cross-section of temperature at 40° N. This SV is representative of the structure of spurious modes.

Fig. 3 Same as Fig. 2, but for the 10th SV. (a) The streamfunction at 500 hPa, and (b)the longitude-model level cross-section of temperature at 45° N.

Fig. 4 The 6th SV of the case where the full physics is included in the linearizations and with an optimal time interval of 36-h. (a) The streamfunction at 500 hPa, and (b) the longitude-model level cross-section of temperature at 1° N.

Fig. 5 Same as in Fig. 4, but for the 8th SV. (a) The streamfunction at 500 hPa, and (b) the longitude-model level cross-section of temperature at 50° N.

Fig. 6 Squared singular values for the leading 10 singular vectors computed (a) using full physics (FP), boundary layer physics (BP) and no physics (NP) versions for the first test case and (b) for the second 12UTC 24 June, 1994 case for full physics (FP) and no moisture (NM).

Fig. 7 The first three SVs of the case where the full physics is included in the linearizations and over an optimization time interval of 24-h.

Fig. 8 Same as Fig. 7, but for 12UTC 24 June, 1994.

Fig. 9 Same as Fig. 8, but the case without moisture (NM).

Table 1: The projection matrix for Case NP and Case BP. The indices on the first row refer to Case NP, and the indices on the first column to Case BP. Each entries m_{ij} of the matrix give the square scalar product between the ith SV of Case NP and jth SV of Case BP, that is, the percentage of energy of ith SV of Case NP explained by the jth SV of Case BP. The last row gives the percentages of energy of ith SV of Case NP by all the 10 SVs of Case BP.

	1	2	3	4	5	6	7	8	9	10
1	78	0	0	0	19	0	0	0	0	0
2	0	0	0	0	0	0	0	0	0	0
3	0	0	36	0	0	33	0	15	0	0
4	0	0	0	0	0	0	81	0	0	0
5	0	0	0	0	0	0	4	0	0	0
6	0	0	27	0	0	49	0	4	0	0
7	0	0	0	0	0	0	0	0	89	3
8	0	0	0	0	0	0	0	0	4	85
9	6	0	0	0	38	0	0	0	0	1
10	0	0	0	0	0	0	0	0	0	4
	85	0	64	0	58	84	85	20	94	94

Table 2: The singular values for Case NP, Case BP, and Case FP. The three singular values with the superscript a denote that their associated SVs have similar structures, and the same meaning holds for b and c.

Cases	Case NP	Case BP	CASE FP
λ_1^2	277	123	9569
λ_2^2	208	38	32
λ_3^2	100	28	$\mathbf{25}^a$
λ_4^2	75	$\mathbf{25}^a$	$\mathbf{22}^b$
λ_5^2	55	24	$\mathbf{21}^c$
λ_6^2	43	23	20
λ_7^2	$\mathbf{29}^a$	$\mathbf{23}^b$	17
λ_8^2	28	$\mathbf{21}^c$	17
λ_9^2	$\mathbf{23}^b$	20	16
λ_{10}^2	$\mathbf{22}^c$	17	15

Table 3: The projection matrix for two FP cases of spatial projection operators for 30°N latitude and the northern Hemisphere. The indices on the first row refer to the case where the spatial projecting operator is defined to include area North of 30°, while the indices on the first column to the case where the spatial projecting operator excludes the southern Hemisphere. Each entry m_{ij} of the matrix gives the square scalar product between the ith SV of the 30° case and jth SV of the northern Hemisphere case, that is, the percentage of energy of ith SV of the 30° case explained by the jth SV of the northern Hemisphere case. The last row provides the percentages of energy of ith SV of the 30° case by all the 10 SVs of the northern Hemisphere case.

	1	2	3	4	5	6	7	8	9	10
1	99	0	0	0	0	0	0	0	0	0
2	0	0	0	98	0	0	0	0	0	0
3	0	0	0	0	97	1	0	0	0	0
4	0	0	0	0	0	0	73	11	13	0
5	0	0	0	0	0	0	0	0	0	87
6	0	0	0	0	0	0	0	1	0	0
7	0	0	0	0	0	0	0	0	0	2
8	0	0	0	0	0	0	0	0	0	0
9	0	0	0	0	0	0	0	0	0	0
10	0	0	0	0	0	0	0	0	0	0
	99	0	0	99	97	2	74	12	14	92

Table 4: The singular values for Case FP and Case NM in the experiments with strong precipitation

Cases	Case FP	CASE NM
λ_1^2	4.9×10^6	9.6
λ_2^2	35.0	9.4
λ_3^2	15.4	8.3
λ_4^2	14.9	7.5
λ_5^2	14.9	7.2
λ_6^2	14.0	7.1
λ_7^2	13.8	6.8
λ_8^2	13.6	6.7
λ_9^2	13.1	6.4
λ_{10}^2	12.3	6.2

Table 5: Singular values for Case FP(full physics) with and without filtering for a time window of 24h for test case 00UTC 03 September 1996

Cases	Case with filtering	CASE without filtering
λ_1^2	410	1932
λ_2^2	6.59	21.0
λ_3^2	6.52	19.8
λ_4^2	6.03	17.1
λ_5^2	5.88	14.3
λ_6^2	5.45	13.2
λ_7^2	5.32	12.5
λ_8^2	4.95	10.9
λ_9^2	4.82	10.5
λ_{10}^2	4.60	8.60

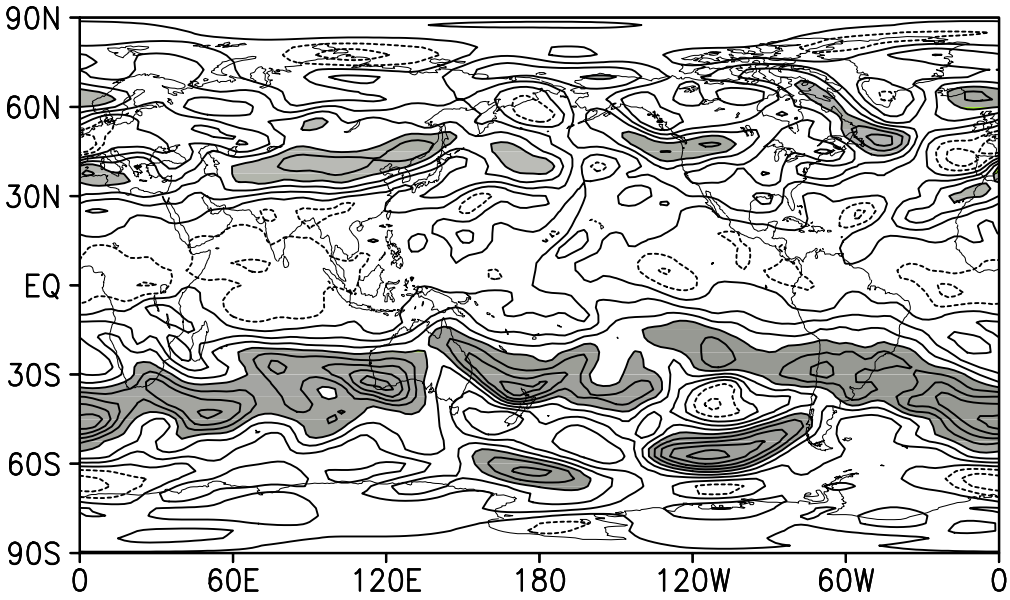
90N
60N
30N
EQ
30S
60S
90S
0
60E
120E
180
120W
60W
0

a)

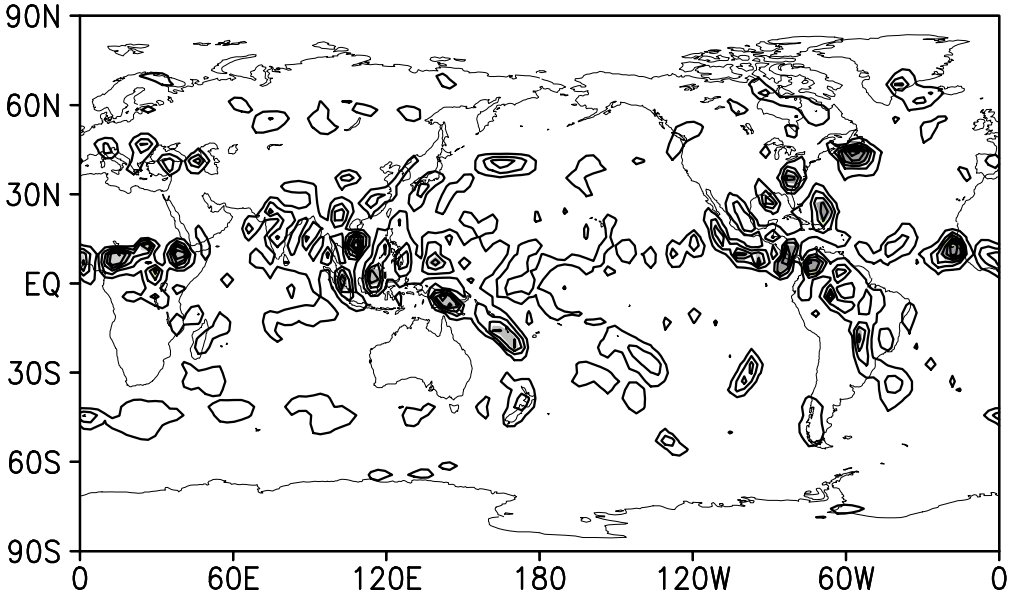
90N
60N
30N
EQ
30S
60S
90S
0
60E
120E
180
120W
60W
0

b)

Figure 1

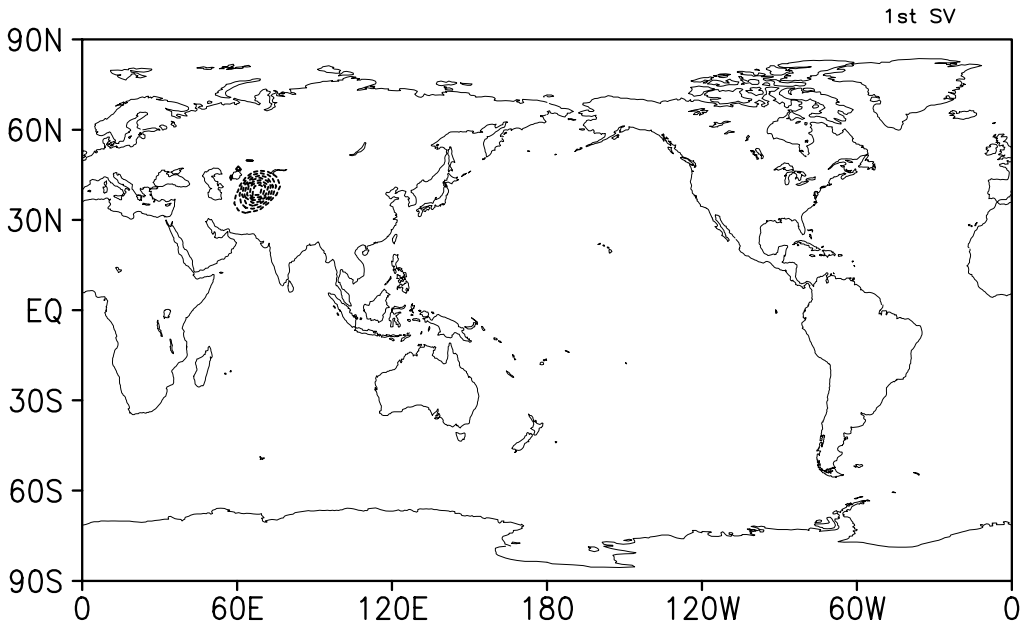
1st SV
90N
60N
30N
EQ
30S
60S
90S
0
60E
120E
180
120W
60W
0

a)

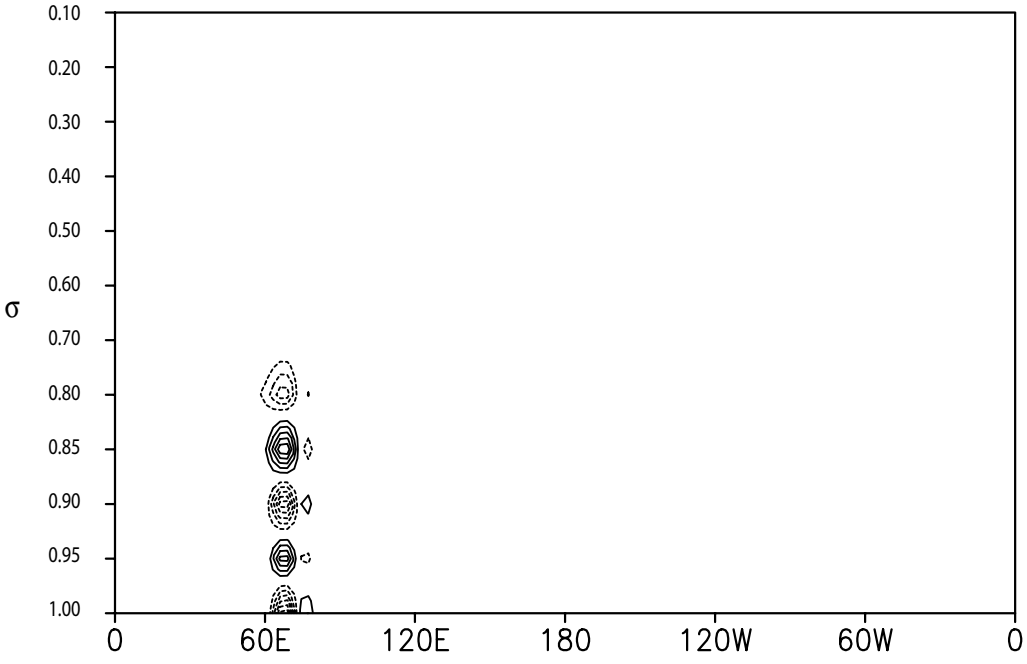
0.10
0.20
0.30
0.40
0.50
0.60
σ
0.70
0.80
0.85
0.90
0.95
1.00
0
60E
120E
180
120W
60W
0

b)

Figure 2

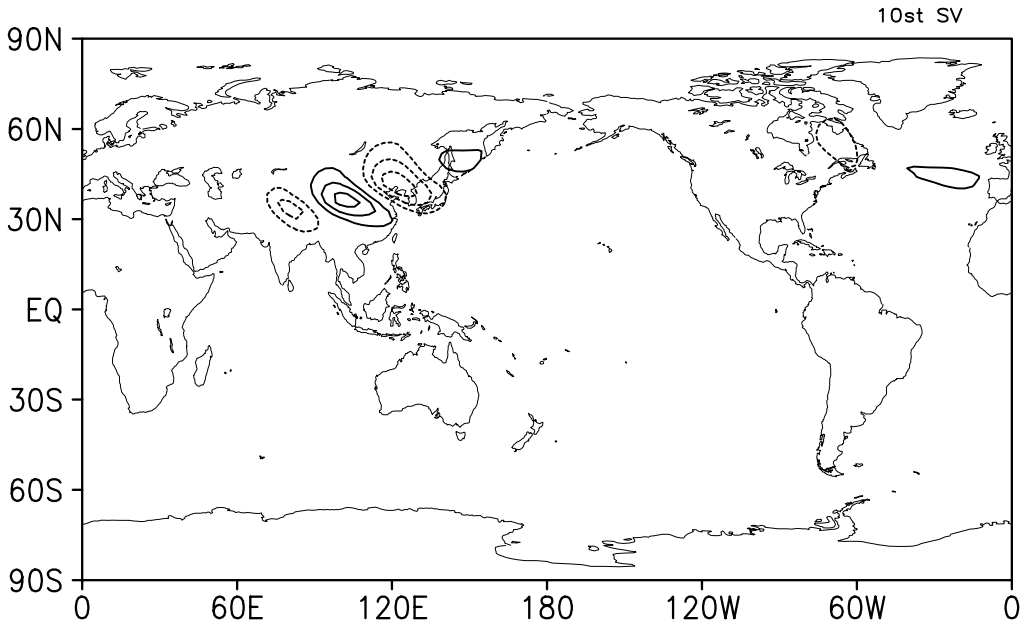
10st SV
90N
60N
30N
EQ
30S
60S
90S
0
60E
120E
180
120W
60W
0

a)

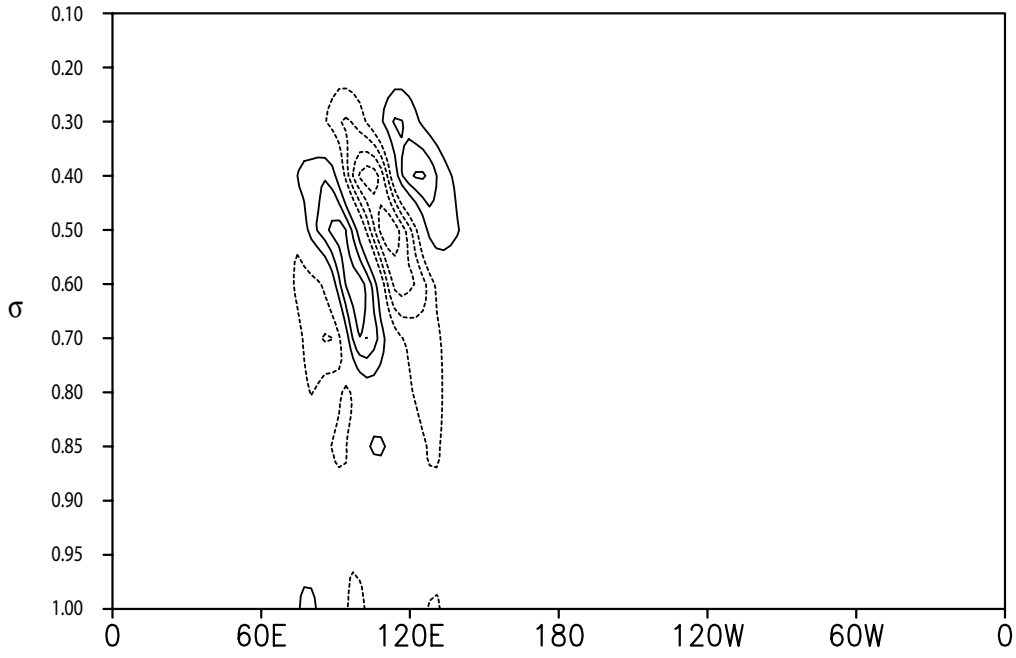
σ
0.10
0.20
0.30
0.40
0.50
0.60
0.70
0.80
0.85
0.90
0.95
1.00
0
60E
120E
180
120W
60W
0

b)

Figure 3

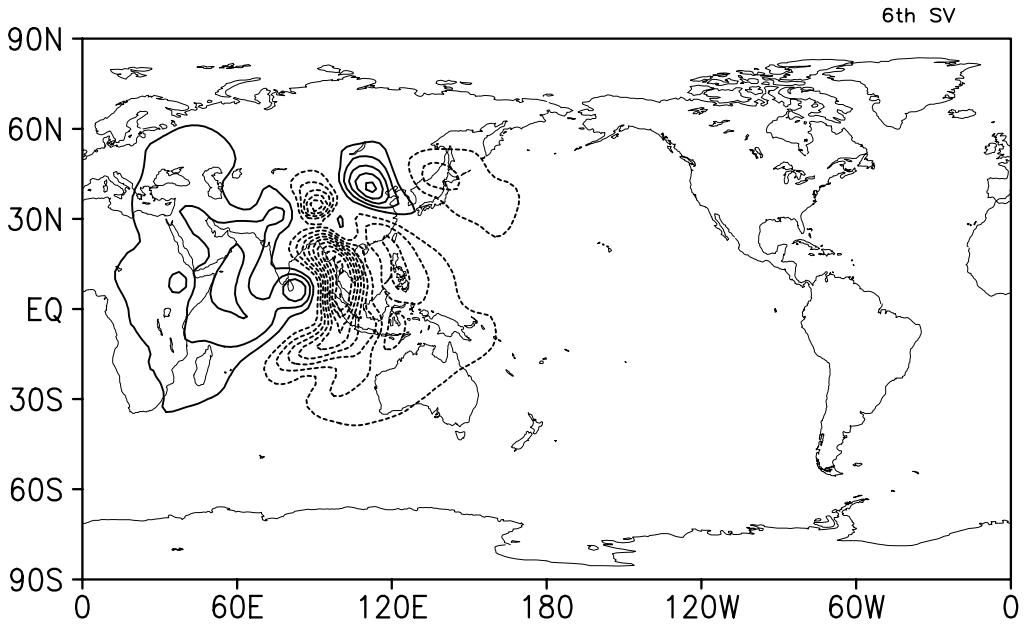
6th SV
90N
60N
30N
EQ
30S
60S
90S
0
60E
120E
180
120W
60W
0

a)

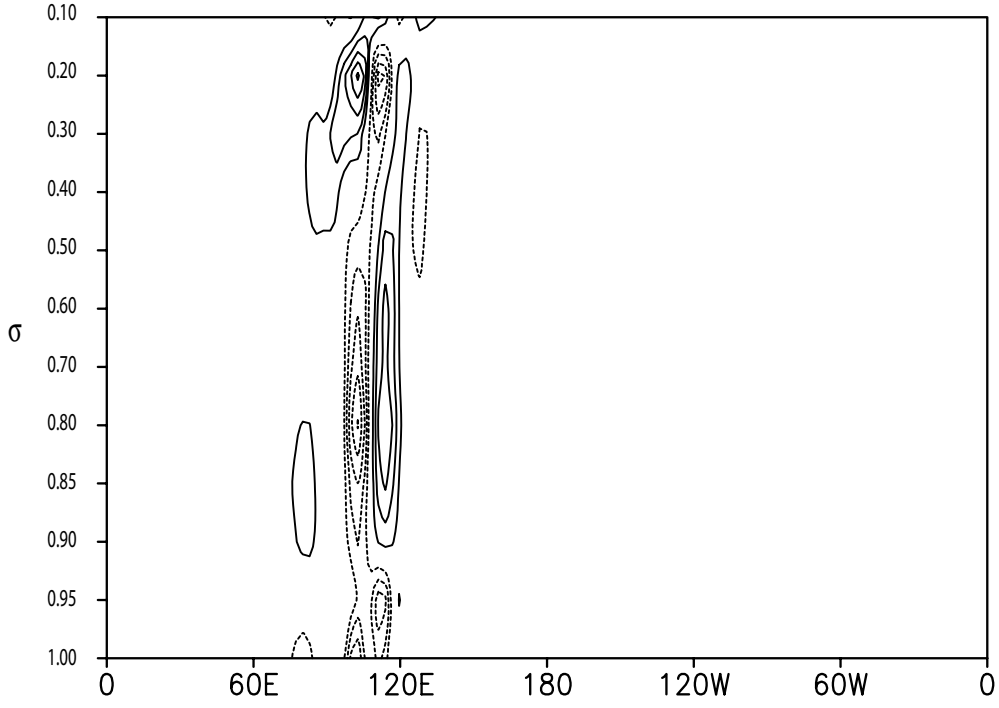
0.10
0.20
0.30
0.40
0.50
0.60
σ
0.70
0.80
0.85
0.90
0.95
1.00
0
60E
120E
180
120W
60W
0

b)

Figure 4

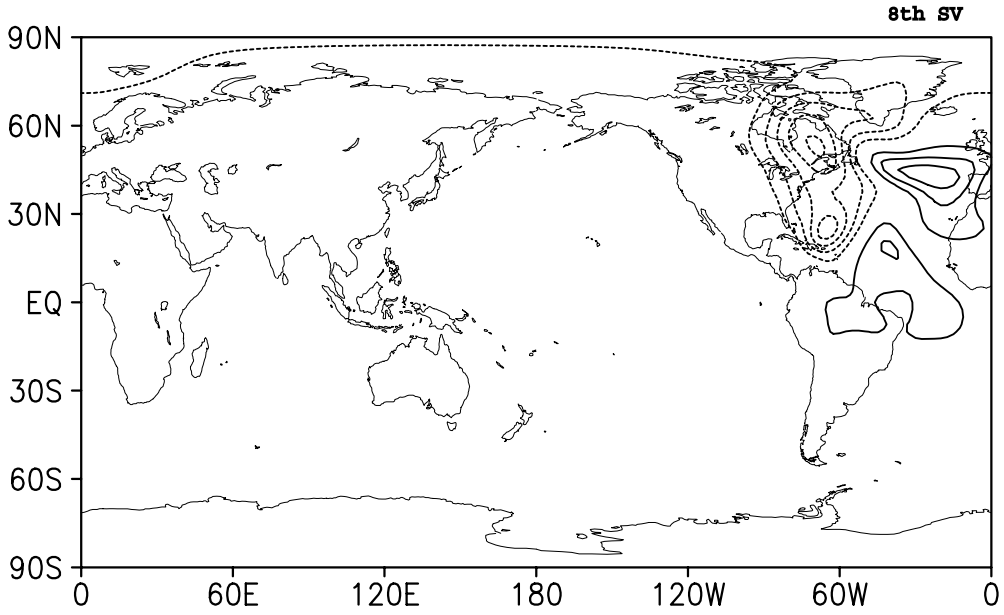
8th SV
90N
60N
30N
EQ
30S
60S
90S
0
60E
120E
180
120W
60W
0

a)

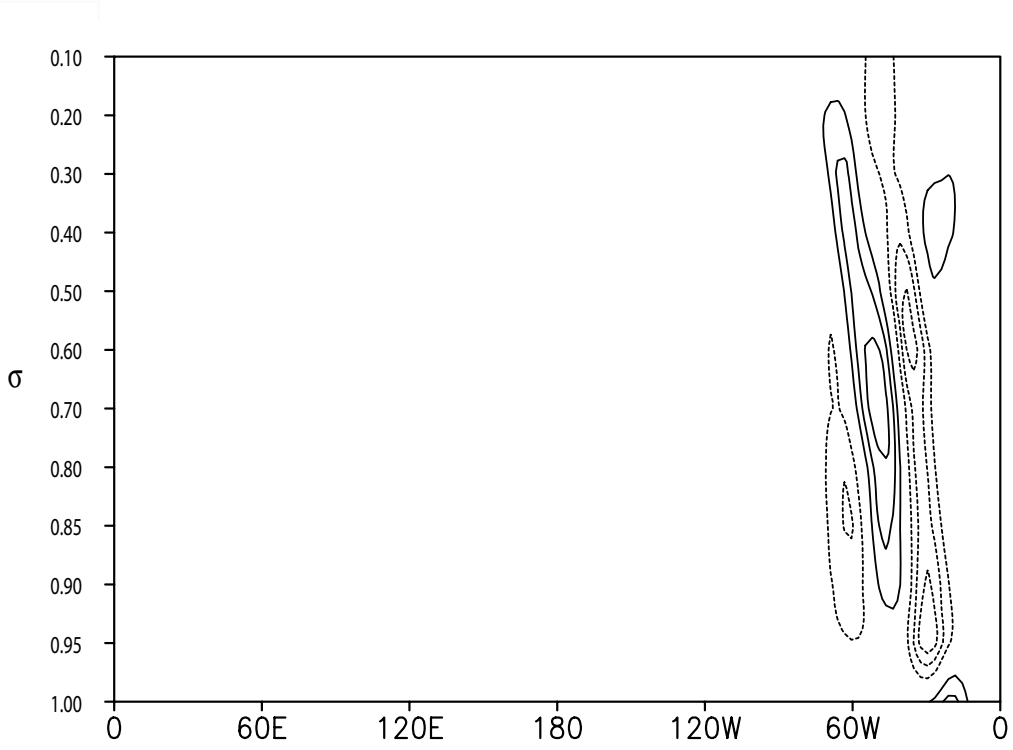
σ
0.10
0.20
0.30
0.40
0.50
0.60
0.70
0.80
0.85
0.90
0.95
1.00
0
60E
120E
180
120W
60W
0

b)

Figure 5

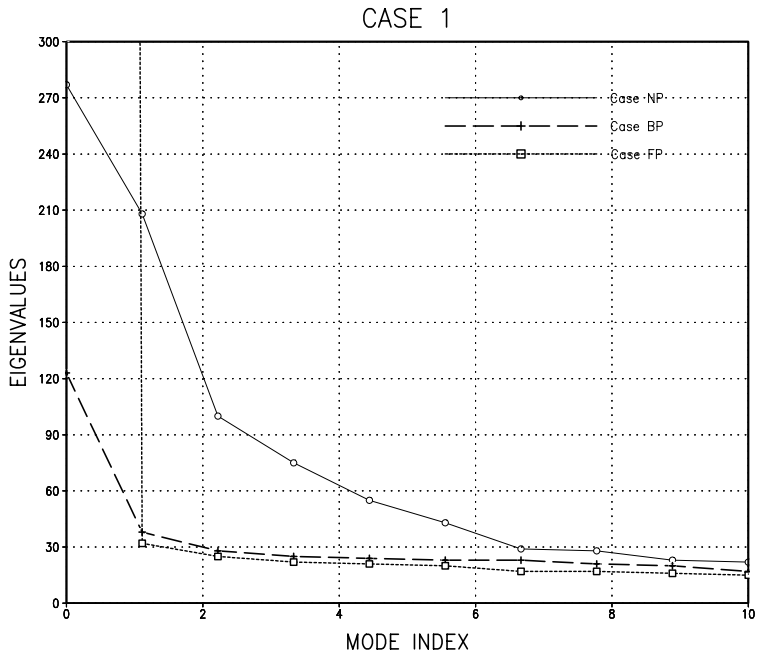
CASE 1
Case NP
Case BP
Case FP
EIGENVALUES
MODE INDEX
0
30
60
90
120
150
180
210
240
270
300
0
2
4
6
8
10

a)

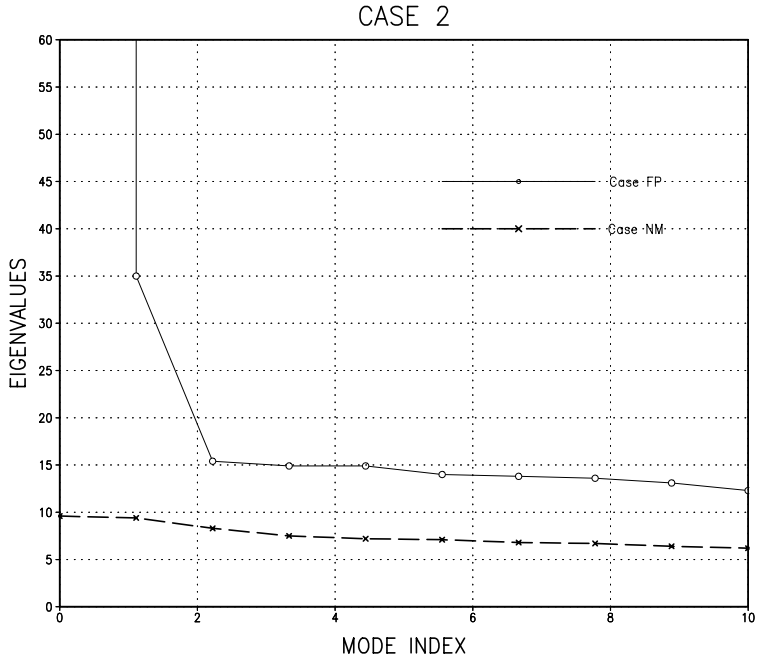
CASE 2
Case FP
Case NM
EIGENVALUES
MODE INDEX
0
5
10
15
20
25
30
35
40
45
50
55
60
0
2
4
6
8
10

b)

Figure 6

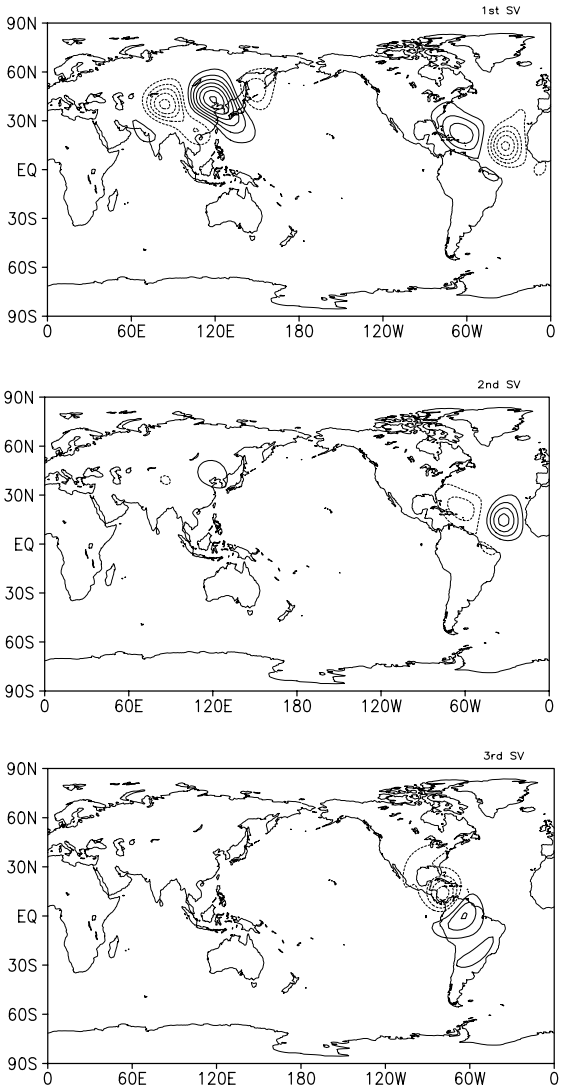
1st SV
2nd SV
3rd SV
90N
60N
30N
EQ
30S
60S
90S
0
60E
120E
180
120W
60W
0

Figure 7

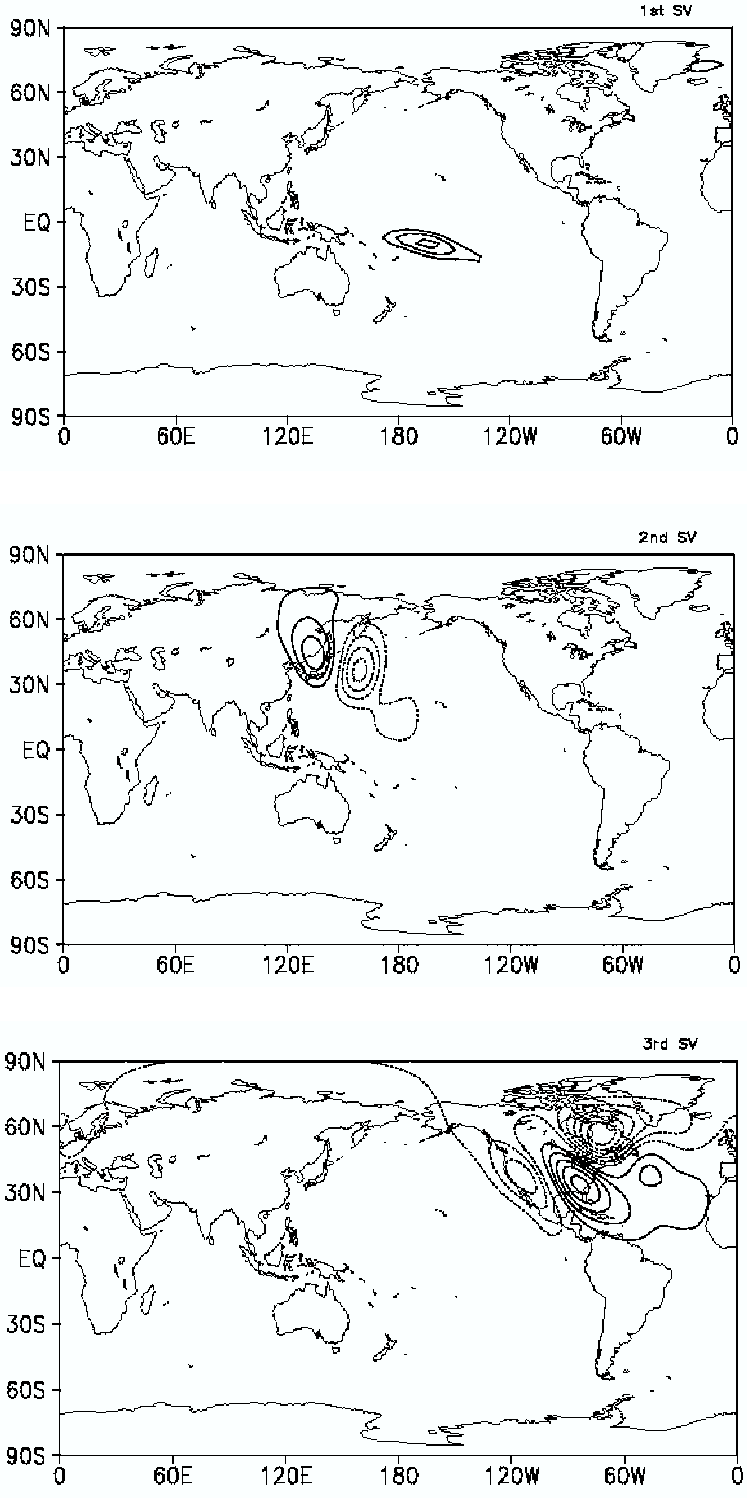
1st SV
2nd SV
3rd SV
90N
60N
30N
EQ
30S
60S
90S
0
60E
120E
180
120W
60W
0

Figure 8

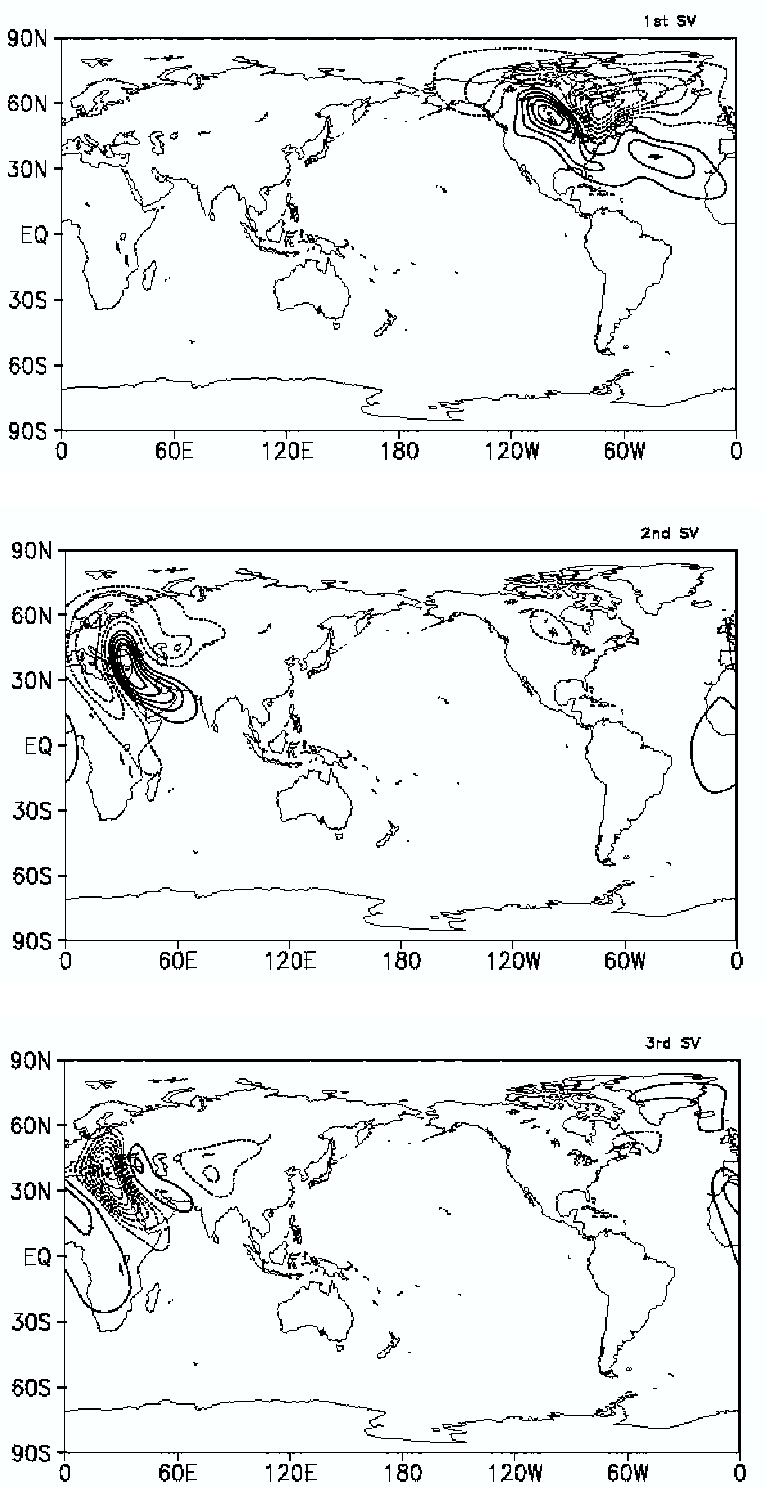
1st SV
90N
60N
30N
EQ
30S
60S
90S
0
60E
120E
180
120W
60W
0
2nd SV
90N
60N
30N
EQ
30S
60S
90S
0
60E
120E
180
120W
60W
0
3rd SV
90N
60N
30N
EQ
30S
60S
90S
0
60E
120E
180
120W
60W
0

Figure 9